Effects of Three-Dimensional Aerodynamics on Blade Response and Loads

Ki-Chung Kim* and Inderjit Chopra†
University of Maryland, College Park, Maryland 20742

A comprehensive rotor aeroelastic analysis based on finite element theory in space and time is coupled with a three-dimensional transonic small disturbance finite difference analysis to investigate three-dimensional aerodynamic effects on blade response and loads in forward flight. Each blade is assumed to be an elastic beam undergoing flap bending, lag bending, elastic twist, and axial deflections. The blade steady response is calculated from nonlinear periodic normal mode equations using a finite element in time scheme. For induced inflow distributions on the rotor disk, a free wake model is used. Dynamic stall and reverse flow effects are also included. Vehicle trim and rotor elastic response are calculated as one coupled solution using a modified Newton method. The blade loads and structural bending are calculated for two blade configurations: a straight-tip blade and a 30-deg swept-back tip blade. Calculated results are correlated with flight-test data obtained from the Gazelle helicopter (with a straight-tip blade) for two level flight speeds. Results then are calculated for this rotor with a swept-tip configuration and the effects of three-dimensional aerodynamics are assessed. Considerable three-dimensional aerodynamic effects are observed in the swept-tip blade.

Nomenclature

C_N	= normal force coefficient
C_T	= rotor thrust coefficient, $T/\rho A(\Omega R)^2$
C_d	= drag coefficient
C_l	= lift coefficient
$C_{m_{ac}}$	= pitching moment coefficient about aerodynamic center
M	= Mach number
N_b	= number of blades
R	= blade radius, m
V	= forward speed, m/s
α	= blade section angle of attack
α_s	= longitudinal shaft tilt (positive for forward tilt)
θ_0	= collective pitch, rad
θ_{1c}, θ_{1s}	= lateral and longitudinal cyclic pitch, rad
μ	= rotor advance ratio, $V/\Omega R$
ϕ_s	= lateral shaft tilt (positive for advancing side up)
Ψ	= rotor azimuth angle, rad
Ω	= rotor rotational speed, rad/s

Introduction

CURRENTLY, most of the rotorcraft codes developed to predict dynamic response and loads in forward flight contain relatively simple aerodynamic modeling compared to the level of sophistication used in structural modeling. A qausisteady two-dimensional aerodynamic approximation is commonly used, and airfoil characteristics are expressed in the form of analytical expressions or tabular data. Uniform or linear inflow is widely used and unsteady aerodynamic effects are represented in an approximate manner. However, the aerodynamic flowfield on a rotor disk is very complex and is coupled with blade motion. For example, the blade encounters transonic flow with shock waves at its advancing blade tip, reverse flow, and stalled flow on its retreating side, and swept flows on its fore and aft positions.

Presented as Paper 89-1285 at the AIAA/ASME/ASCE/AHS/ASC 30th Structures, Structural Dynamics and Materials Conference, Mobile, AL, April 3-5, 1989; received Aug. 24, 1989; revision received July 2, 1990; accepted for publication Aug. 8, 1990. Copyright © 1989 by the American Institute of Aeronautics and Astronautics, Inc. All rights reserved.

*Research Assistant; currently Post-Doctoral Fellow, Department of Aerospace Engineering. Member AIAA.

†Professor, Department of Aerospace Engineering. Fellow AIAA.

Recently, there have been some limited attempts to refine the three-dimensional aerodynamic effects in the calculation of blade response and loads. In Refs. 1 and 2, the authors coupled finite-difference aerodynamic codes and rotor dynamic codes in a loose manner to predict structural bending and aerodynamic loads on an advanced geometry rotor blade. The dynamic codes were used to predict angle-of-attack distribution and variation on the rotor disk for a trimmed condition and then, using this information, the finite-difference codes calculated the detailed flowfield including formation of shocks on the advancing blade tips. From the correlation of predicted results with flight-test data, it was shown that the three-dimensional aerodynamics had a considerable influence on blade dynamic response and loads, in particular at high forward speeds. In both Refs. 1 and 2, only the three-dimensional lift was included, and the three-dimensional pitching moment was not included. However, it is well known that blade pitching moment characteristics play an important role on the torsional dynamics of the blade, more so for a torsionally soft rotor. Also, in earlier studies the control settings were not updated when using the three-dimensional aerodynamics, which might influence the trim state of the rotor. In the present study, the rotor response as well as rotor controls are calculated using three-dimensional aerodynamics and both the three-dimensional lift and pitching moment are included in the coupled analysis.

Also, in the present study, the analysis is further extended to study the dynamics of a rotor blade with swept tip, where the three-dimensional aerodynamic effects can be quite significant. Recently, Celi and Friedman[3] and Benquet and Chopra[4] studied the dynamics of a swept-tip rotor by incorporating a proper structural modeling for the tip. In Ref. 3, authors showed that frequently used equivalent sweep model (representing the tip element in terms of chordwise shift of aerodynamic center and center of gravity) can lead to a considerable deviation in results from those obtained using refined sweep model. Both papers used quasisteady aerodynamics and linear transformation relations between blade and tip elements. In the present paper, a refined dynamic analysis of swept-tip rotors in forward flight is formulated, including detailed three-dimensional aerodynamics and nonlinear transformation relations between blade and tip elements.

Results are first calculated for an advanced geometry rotor with a straight tip and correlated with the flight-test data.[5] The data was obtained by Aerospatiale on a SA349/2 Gazelle

helicopter dedicated to experimental research. It was an advanced geometry three-bladed articulated rotor. Results then are calculated for this rotor with a swept-tip configuration and the effects of three-dimensional aerodynamics are assessed. The three-dimensional effects on blade response and loads are discussed in terms of rotor controls, elastic blade response, structural bending, and lift and pressure distribution. Formulation details and several other correlations and parametric studies are available in Ref. 6.

Formulation

Rotor Dynamic Analysis

The baseline rotor dynamic analysis is a comprehensive aeroelastic analysis based on finite-element theory in space and time.[7-11] The blade is assumed to be an elastic beam undergoing flap bending, lag bending, elastic twist, and axial deflections. Each blade is discretized into a number of beam elements and for each element there is a continuity of displacement and slope for flap and lag deflections, and a continuity of displacement for axial and torsion deflections. There are two internal nodes for axial displacement and one for elastic twist resulting in a total of 15 degrees of freedom for each element. The formulation for the blade equations of motion is based on Hamilton's principle. The analysis is developed for a nonuniform blade having pretwist, precone, and chordwise offsets of the center of mass, aerodynamic center, and tension center from the elastic axis.

Recently, the analysis was extended to model the advanced-tip rotor, including swept and anhedral tips, for small angles.[4] In the present paper, the analysis is further refined for swept tips with large angles. In order to model the blade with a tip sweep, special considerations are needed in the assembly of a straight element and a swept element. It is assumed that the geometric angle at the interface between the straight element and the swept-tip element is preserved before and after deformation. In the assembly of elements, suitable compatibility conditions are introduced at the interface for moderate rotations. Inertial and aerodynamic characteristics of the tip element are modified to include effects of sweep angle.[12]

Aerodynamic loads for the dynamic analysis are calculated using quasisteady strip theory. Noncirculatory aerodynamic forces are also included. To include the effect of high angle-of-attack flows, a dynamic-stall model proposed by Johnson[13] is incorporated. Dynamic stall characterizes the delay in flow separation due to unsteady angle of attack, and the shedding of a vortex from the leading edge of the airfoil when it gets into a deeper stall condition. These effects are introduced in the calculation of section lift, drag, and pitching moment. For this, the time history of blade motion of the previous cycle is used.

Aerodynamic coefficients are computed in the form of analytical expressions as well as data tables. These are represented as

$$\begin{aligned} C_l &= c_0(\alpha,M,q,\dot{q}) + c_1(\alpha,M,q,\dot{q})\alpha \\ C_d &= d_0(\alpha,M,q,\dot{q}) + d_1(\alpha,M,q,\dot{q})\alpha \\ &\quad + d_2(\alpha,M,q,\dot{q})\alpha^2 \\ C_{m_{ac}} &= f_0(\alpha,M,q,\dot{q}) + f_1(\alpha,M,q,\dot{q})\alpha \end{aligned} \tag{1}$$

where q and $\dot{q}$ are arrays of nodal displacements and velocity vectors, respectively. Equation (1) represents a set of nonlinear aerodynamic coefficients including effects of blade motion and Mach number.

The rotor response analysis consists of two phases, vehicle trim and steady response, and both are calculated as one coupled solution using a modified Newton method.

Vehicle Trim

Propulsive trim, which simulates a free-flight condition of the vehicle, is used to calculate rotor control settings. The solution is determined from vehicle overall nonlinear equilibrium equations: three force (vertical, longitudinal, and lateral), and three moment (pitch, roll and yaw) equations. For a specified weight coefficient C_w and forward speed μ, the trim solution evaluates the shaft tilt angles (α_s, ϕ_s), the pitch control settings (θ_0, θ_{1c}, θ_{1s}), and the tail rotor thrust.

These trim values are recalculated iteratively using the modified hub forces and moments including the blade elastic responses and three-dimensional aerodynamic effects.

Steady Response

The steady response involves the determination of time-dependent blade positions at different azimuth locations for one rotor revolution. To reduce computational time, the finite-element equations are transformed into modal space as a few normal mode equations using the coupled natural vibration characteristics of the blade. These nonlinear periodic coupled equations are solved for steady response using a finite element in time procedure based on Hamilton's principle in weak form. One rotor revolution is divided into a number of azimuthal elements and then periodicity of response is used to join the motions of the first and last elements. The assembly of elements results in nonlinear algebraic equations, which are solved using the Newton-Raphson procedure (for detail, see Ref. 11).

After the blade response is obtained, structural bending moments at different spanwise positions are calculated using the modal method.

Rotor Wake Modeling

For the induced inflow distribution on the rotor disk, a free wake model[14] is fully coupled in the rotor aeroelastic analysis. The model can account for its self-distortion by updating its geometry according to newly calculated inflow and blade circulation. The geometry of the free wake is divided into three regions; near wake, rolling-up wake, and far wake. The near wake consists of a series of radial panels, each with linear circulation distributions. The rolling-up wake consists of an inboard linear circulation distribution panel, and a tip panel that represents the rolling up of the tip vortex. The far wake is modeled as one panel of linear circulation distribution, and a concentrated tip vortex whose strength is proportional to the maximum circulation value on the rotor blade. The helical geometry of the concentrated tip vortex is updated while the inboard wake portions are not changed.

The free wake analysis is implemented in three stages. First, blade motion and loading are calculated using a linear inflow model. Next, wake-induced coefficients are calculated for an undistorted wake geometry. The nonuniform inflow is calculated and is used to obtain blade motion and loading. Finally, the free wake geometry is calculated. For this, the influence coefficients are re-evaluated, and blade motion and loading are again obtained using nonuniform inflow values. For subsequent iterations, the free wake geometry is generally held fixed, and only the strength of vortices are updated.

For the calculation of three-dimensional aerodynamics, the influence of the near wake (up to 5 chords behind the blade) in the free wake model is suppressed since it is calculated as a part of the finite-element difference grid solution.

Finite Difference Three-Dimensional Aerodynamic Analysis

A finite-difference aerodynamic analysis based on three-dimensional unsteady transonic small disturbance theory is used to calculate the flowfield around the rotor blade.[15] The method is able to treat nonlinear flowfields associated with unsteady transonic flows occurring at advancing blade tips at high forward speeds. It can analyze blades of arbitrary planforms using the grid mapping procedure.

Initially, the classical unsteady transonic small disturbance equation was used. Later, a modification was introduced into the analysis to extend the domain of validity to large cross flows and larger azimuthal sectors.[16] This modification enhanced the computational efficiency as well as the numerical stability of solution procedure for nonrectangular blade planforms. This uncoupled aerodynamic code has been extensively used to calculate detailed flowfields on rotor blades including advanced tip shapes, and to correlate the computed results with measured data from model rotors.[17,18]

In the present paper, the finite-element dynamic analysis is coupled with the finite-difference aerodynamic analysis in an iterative manner. This coupled analysis is then used to calculate three-dimensional effects as well as transonic flow with shock waves on advancing blade tips for both straight-tip and swept-tip blades. The modification for a swept-tip blade in the three-dimensional finite-difference aerodynamic analysis is modeled by the coordinate transformation. Time history of the angle-of-attack distribution, obtained from the rotor aeroelastic code, is used as input data for this finite-difference code.

Solution Procedure

To improve the efficiency of the coupled analysis, three-dimensional C_l and C_m are used for the outer 50% of the blade on the advancing side and for the outer 20% on the retreating side. The following procedure was used to couple the rotor aeroelastic analysis with the finite-difference three-dimensional aerodynamic analysis.

1) With prescribed input data, a vehicle uncoupled trim is calculated using two-dimensional aerodynamic tables.

2) Using control inputs from the vehicle trim solution of step 1, the blade nonlinear steady response is calculated. Again, two-dimensional aerodynamic tables are used to obtain the aerodynamic coefficients at different radial stations and azimuthal positions.

3) Hub loads and moments are calculated using elastic rotor response. Then, the vehicle trim values and blade responses are recalculated iteratively using the modified hub forces and moments. This step is repeated until a converged solution is obtained.

4) Using the calculated effective angle-of-attack distribution from step 3, the finite-difference solution is computed. The results give detailed pressure distributions on the blade (spanwise and chordwise) at different azimuthal positions along with three-dimensional C_l and C_m.

5) First, only three-dimensional C_l is included in the coupling process along with two-dimensional C_m. Steps 3 and 4 are repeated until the finite-difference solution and rotor responses are converged for three-dimensional C_l.

6) Then, the three-dimensional C_m is included along with the converged three-dimensional C_l value. For this, the three-dimensional C_l value is held fixed and steps 3 and 4 are repeated until a converged solution is obtained. Finally, rotor controls, blade response and loads are recomputed using both three-dimensional C_l and C_m.

Table 1 SA349/2 Helicopter characteristics

Aircraft gross weight	4400 lbs
Number of blades, N	3
Radius, R	5.25 m
Blade chord, c	0.35 m
Solidity, σ	0.064
Lock number, γ	5.13
C_T/σ	0.067 (μ = .14) 0.064 (μ = .378)
Airfoil	OA209
Rotational speed, Ω	387 rpm
Rotating flap natural frequency	1.02/rev
Rotating lag natural frequency	0.54/rev
Rotating torsion natural frequency	3.72/rev
Fuselage lift coefficient, C_{L_f}	0.00499
Fuselage drag coefficient, C_{D_f}	0.0092
Fuselage pitch moment, C_{pm}	−0.00086
Fuselage roll moment, C_{rm}	−0.0001
Fuselage yaw moment, C_{ym}	0.0001

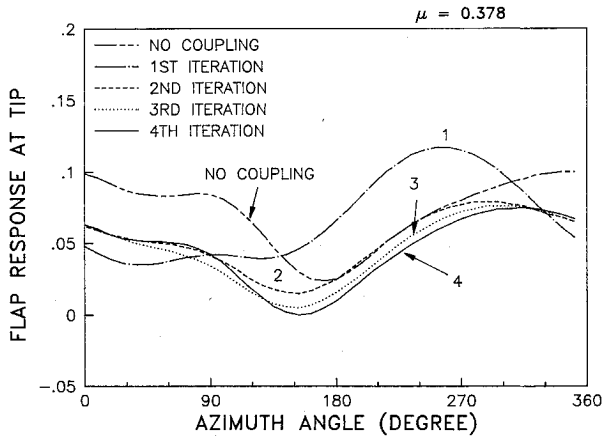

Fig. 1 Convergence study of the coupled analysis.

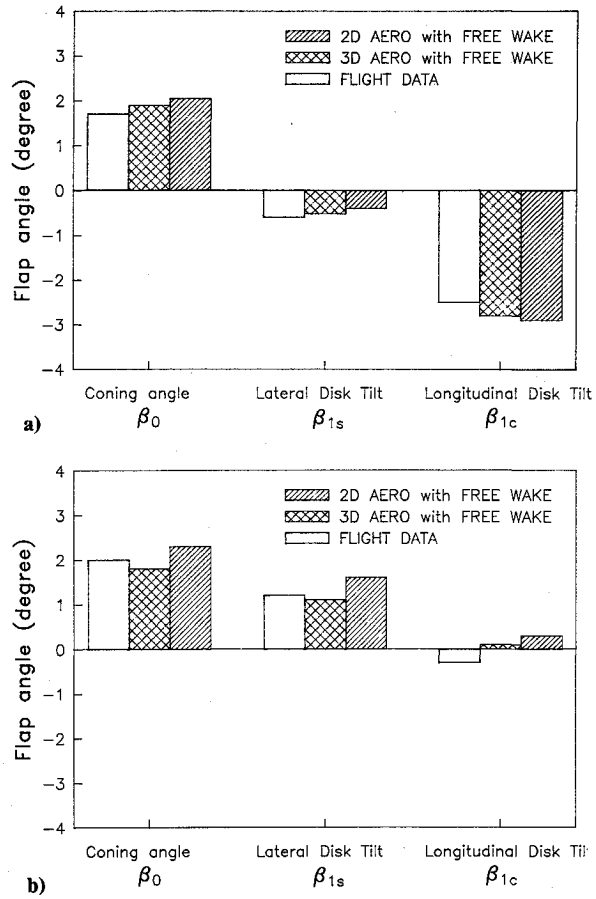

Fig. 2 Correlation of flap response at blade tip: a) Low forward speed (μ = 0.14); b) High forward speed (μ = 0.378).

Results and Discussion

Results are first calculated and correlated for a straight-tip three-bladed rotor of the SA349/2 Gazelle helicopter for level flight conditions at two different flight speeds, 30 m/s (μ = .14) and 80 m/s (μ = .378). Results then are calculated for this rotor with a 30-deg swept-tip configuration and the effects of three-dimensional aerodynamics are assessed. Some important structural and aerodynamic characteristics of this rotor are shown in Table 1. Other characteristics are given in Ref. 5.

Table 2 Correlation of trim controls

	$\mu = 0.14$, $C_T/\sigma = 0.067$			$\mu = 0.387$, $C_T/\sigma = 0.064$		
Pitch angle	Flight data	Two-dimensional aero free wake	Three-dimensional aero free wake	Flight data	Two-dimensional aero free wake	Three-dimensional aero free wake
θ_0	6.93	5.58	5.78	14.42	14.29	14.92
θ_{1c}	1.45	0.54	0.57	2.21	1.53	1.74
θ_{1s}	1.04	1.23	1.25	−9.35	−8.8	−8.61

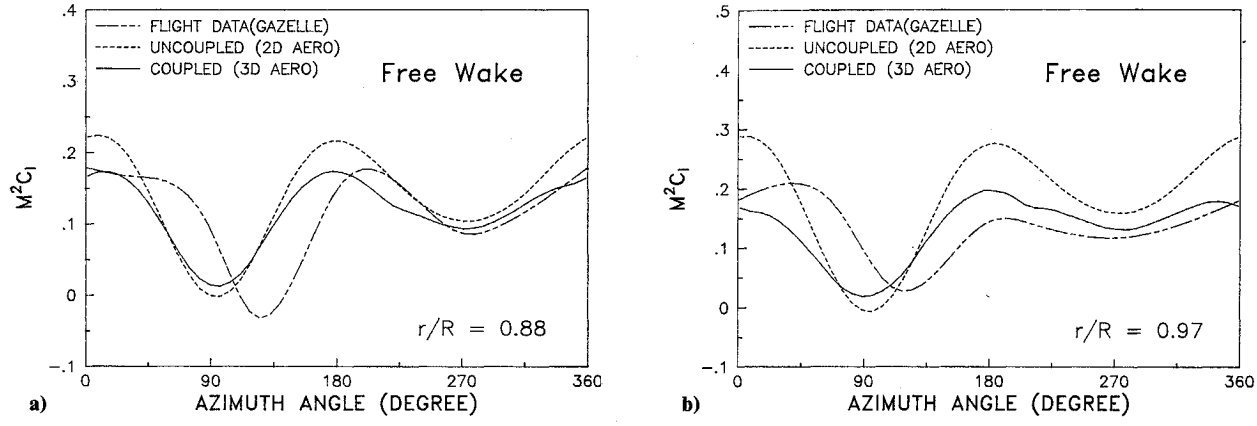

Fig. 3 Correlation of lift coefficients ($\mu = 0.378$): a) Radial station at $0.88R$; b) Radial station at $0.97R$.

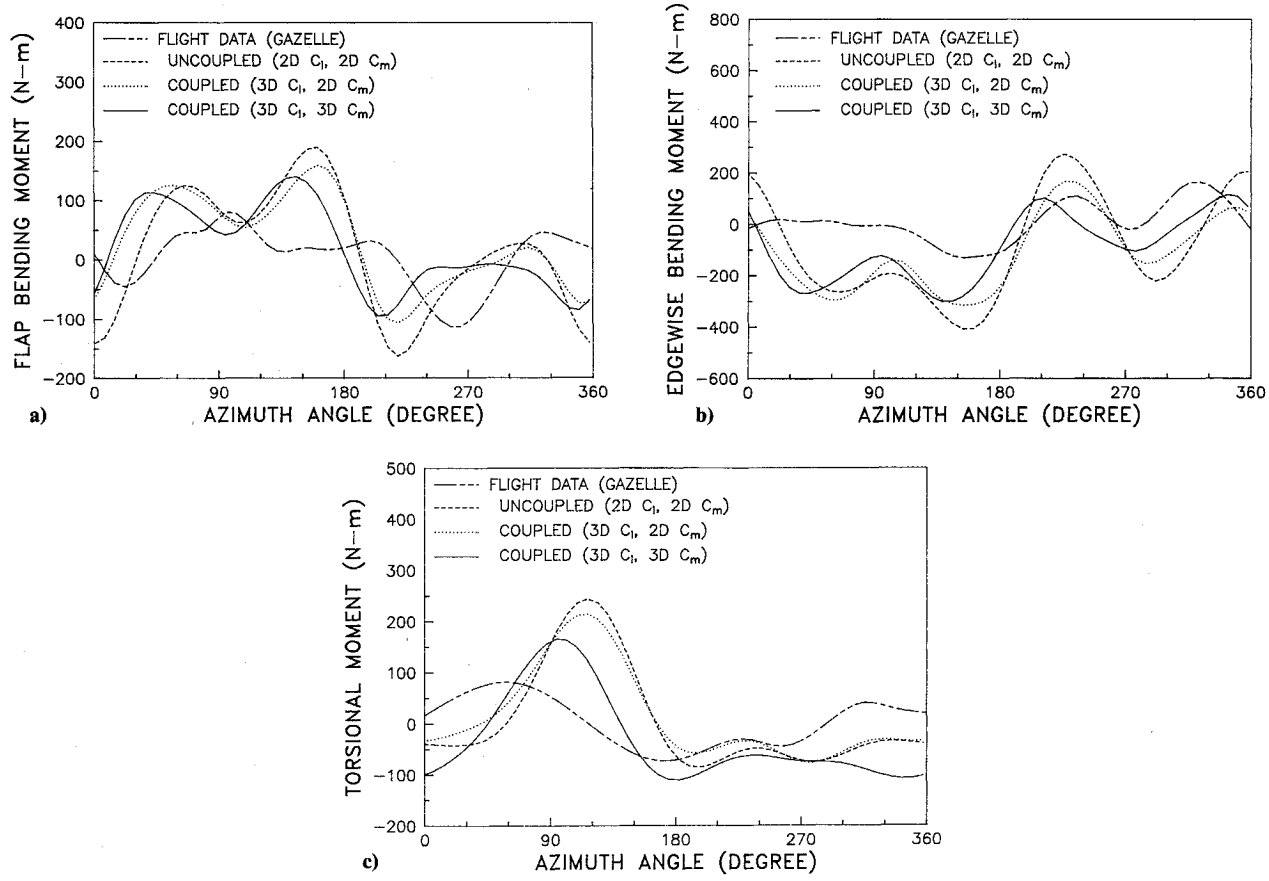

Fig. 4 Correlation of structural bending moments ($\mu = 0.378$): a) Flap bending moment at $0.8R$; b) Lag bending moment at $0.8R$; c) Torsional moment at $0.8R$.

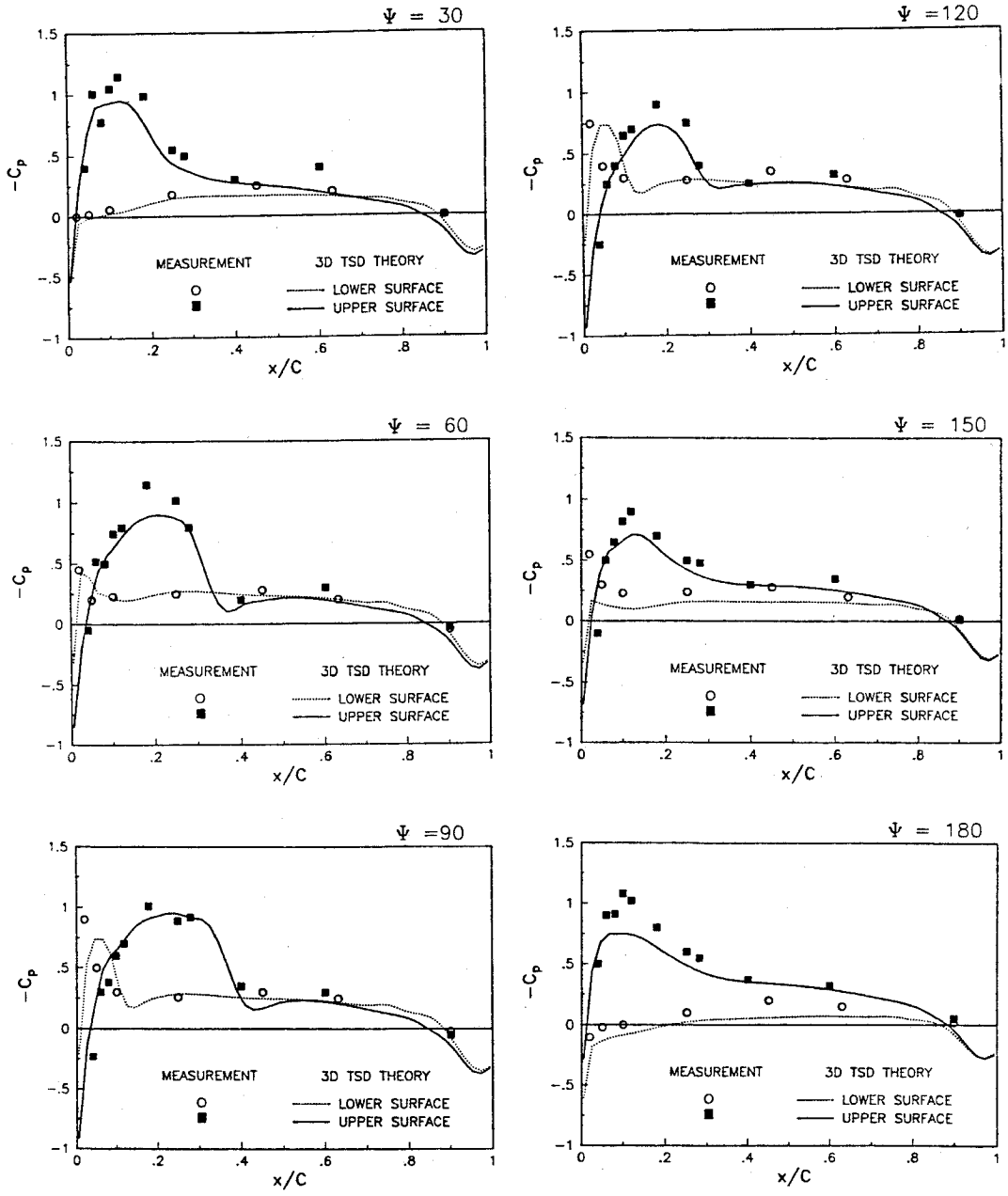

Fig. 5 Correlation of pressure distributions at 0.97R (μ = 0.378).

For the calculation of blade response, the blade is discretized into eight beam elements and each beam element consists of fifteen nodal degrees of freedom. For normal mode reduction, eight coupled rotating natural modes are used, comprised of three flap, two lag, two torsion and one axial modes. For periodic response, one revolution is discretized into eight time elements and each time element represents a fifth-order-polynomial distribution of motion. These approximations appear to yield satisfactory converged results (four significant digits).

To investigate the three-dimensional transonic aerodynamic effects on dynamic response, three-dimensional lift and moment coefficients calculated from the finite-difference code are included in the dynamic code. The convergence study of coupling of dynamic and aerodynamic codes is shown in Fig. 1. It shows flap response at the blade tip for one rotor revolution at a high speed flight condition (μ = .378). First, the dynamic blade response and loads are calculated using quasisteady aerodynamics and two-dimensional data tables (without coupling). Using the angle-of-attack distribution from the aeroelastic code as input, three-dimensional finite-difference aerodynamics is computed. Then, with three-dimensional lift distributions from the computational fluid dynamics (CFD) code, the dynamic response and the rotor controls are recomputed until converged solutions are obtained (indicated by the first iteration curve in Fig. 1). For subsequent iterations, updated angle-of-attack distributions from the aeroelastic code are used. It is observed that the coupled solution converges after three iterations for three-dimensional lift. After the convergence in lift is achieved, then the three-dimensional C_m is included in the coupling process along with converged three-dimensional C_l. It is also found that two iterations are sufficient for achieving the convergence in three-dimensional C_m. After the fourth iteration, the variation in tip flap response is quite negligible and therefore is not presented.

Straight-Tip Blade

Calculated vehicle trim values are correlated with the flight data in Table 2 for two level flight conditions, a low speed (μ = 0.14) and a high speed (μ = 0.378). The predicted and measured results agree very well for collective pitch, but there is a slight disagreement for the cyclic pitch angles. The calcu-

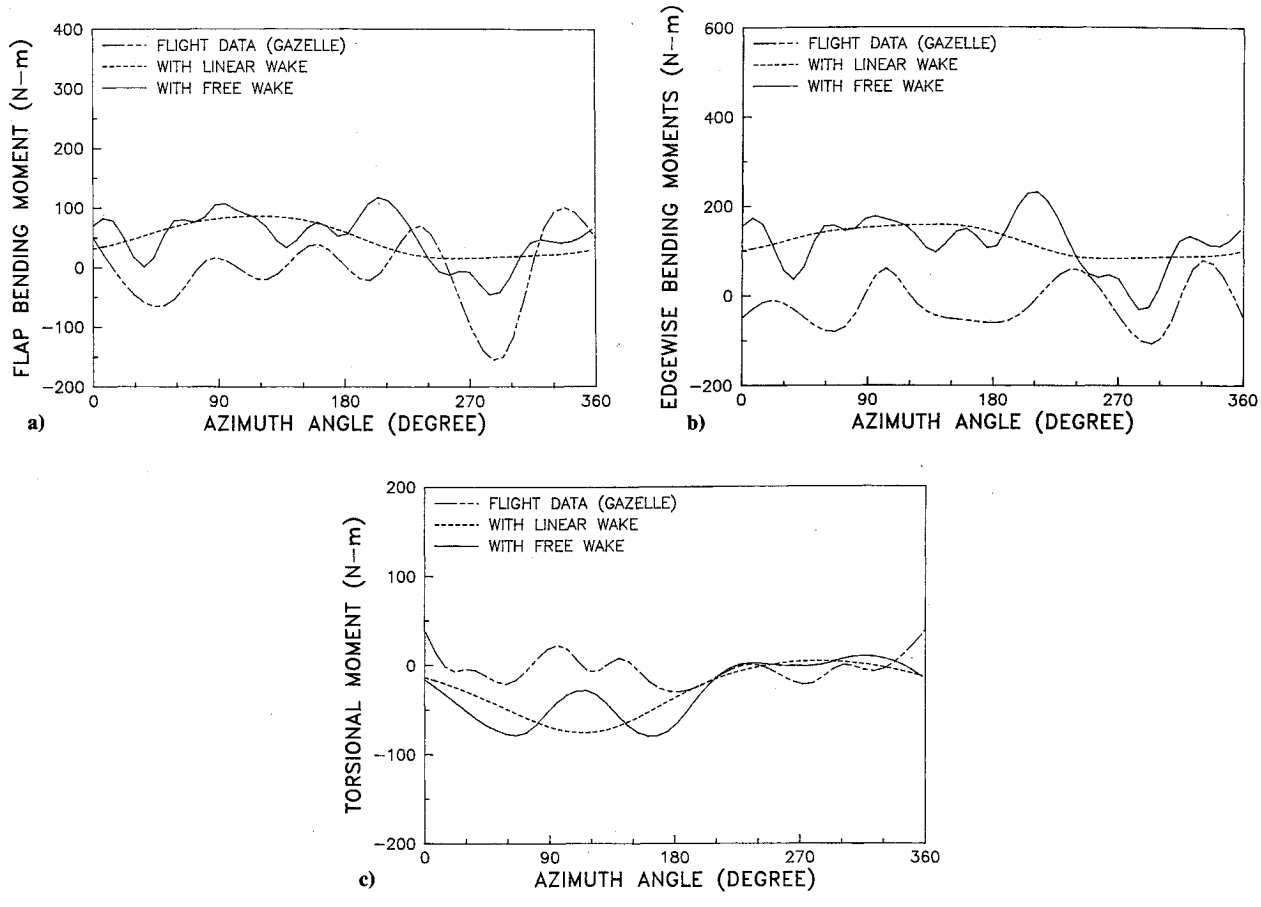

Fig. 6 Correlation of structural bending moments ($\mu = 0.14$): a) Flap bending moment at $0.8R$; b) Lag bending moment at $0.8R$; c) Torsional moment at $0.8R$.

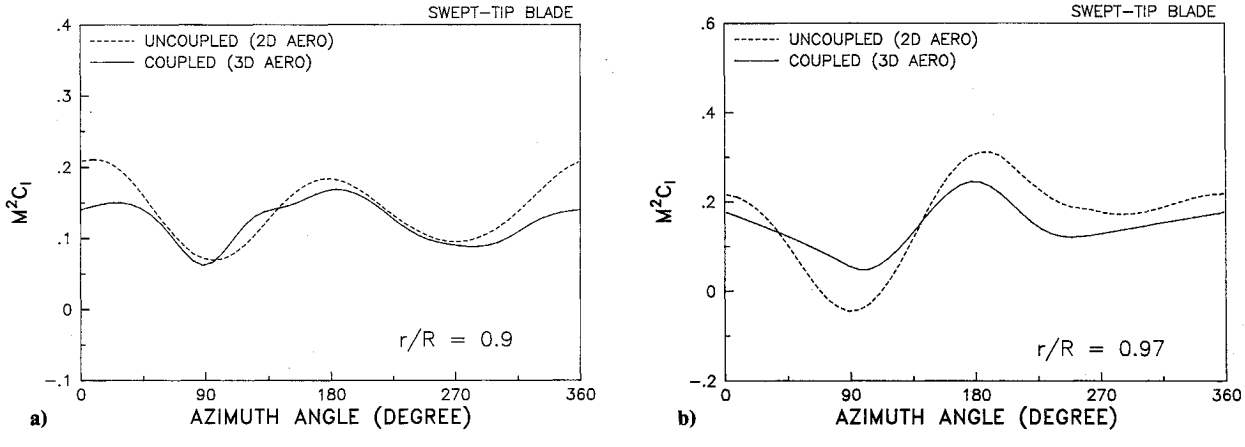

Fig. 7 Lift variations of swept-tip blade ($\mu = 0.378$, tip sweep = 30 deg, outer 10% R): a) radial station at $0.9R$; b) Radial station at $0.97R$.

lated collective pitch angle with three-dimensional aerodynamics is higher than the one calculated with two-dimensional aerodynamics, and improves the correlation. To achieve the desired thrust, more collective pitch setting is needed with three-dimensional aerodynamics because of reduced lift at the tips. For the high-speed case, including the three-dimensional aerodynamic effects in coupled trim solution helps the lateral cyclic pitch correlation. This improvement is most likely due to the fact that the transonic condition occurring at the advancing blade tip is well represented in the three-dimensional aerodynamic modeling.

Calculated flap angles are correlated with the flight data in Fig. 2. Analytical results using two-dimensional quasisteady aerodynamics with the free wake and the three-dimensional aerodynamics (three-dimensional C_l, C_m) with the free wake are presented along with test values. For the high-speed condition, flap response obtained using the three-dimensional aerodynamics shows better agreement with the test data than using the two-dimensional aerodynamics. For β_0, the three-dimensional value is smaller than the two-dimensional value because of reduced lift at the tips. Noticeable improvements in predicting the disk tilts (β_{1s} and β_{1c}) with three-dimensional aerodynamics are observed for the high-speed case ($\mu = 0.378$).

High Forward Speed ($\mu = 0.378$)

In this section, results are calculated for the high-speed level flight condition, where large three-dimensional effects are expected. A thrust level C_T/σ of 0.064 is used. As expected for this high-speed condition, the results obtained using the free

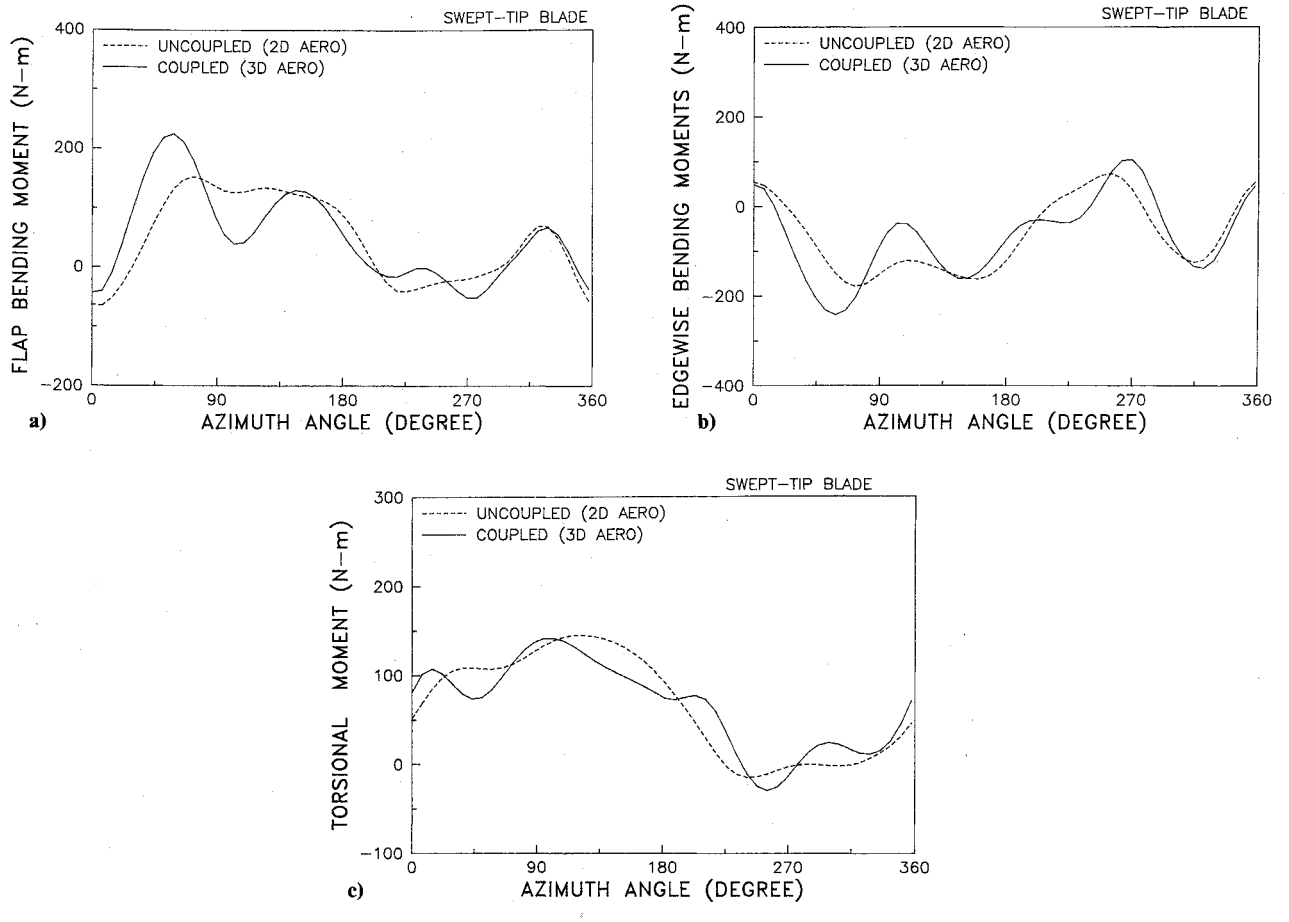

Fig. 8 Structural bendings of swept-tip blade ($\mu = 0.378$, tip sweep = 30 deg, outer 10% R): a) Flap bending moment at $0.8R$; b) Lag bending moment at $0.8R$; c) Torsional moment at $0.8R$.

wake model are similar to those obtained using the linear wake model (Drees), and therefore, results obtained with the free wake model are presented only.

Figure 3 shows the lift coefficient variation (in terms of nondimensional lift, M^2C_l) for two radial stations located respectively at 88% and 97% of the radius. For comparison, the uncoupled dynamic code (two-dimensional aero) and the coupled code (three-dimensional aero) are presented together with the flight-test data. It is observed that three-dimensional effects are quite significant and correlation with data improves with inclusion of three-dimensional aerodynamics.

Structural bending moments at the 80% radial station are plotted in Fig. 4. For comparison, three sets of analytical results are plotted along with the flight data: results with two-dimensional-C_l and two-dimensional-C_m, with three-dimensional-C_l and two-dimensional-C_m, and three-dimensional-C_l and three-dimensional-C_m. Flap bending, lag bending and torsional moment variation with azimuth angle are determined using a modal approach. There are some differences between two analytical results obtained using three-dimensional aerodynamic effects. Including three-dimensional effects in pitching moment shows significant differences and helps to improve the correlation for torsional moment. Considering the fact that mean values of bending moment in data were not available, the overall correlations appear satisfactory.

Comparison between the measured chordwise pressure distributions and the calculated results obtained from the three-dimensional finite-difference code are shown in Fig. 5 for a station near the tip (.97R). Generally, good agreement between predicted and measured pressure distributions are observed in almost all azimuthal locations. Also, the shock appearances on the upper surface of the blade, particularly around 60- and 90-deg azimuthal position, are well captured.

Low Forward Speed ($\mu = 0.14$)

Results are obtained for a low-speed level flight condition (1g) with thrust level C_T/σ of 0.067. Lift and response variation results along azimuth showed that there is only a slight effect of three-dimensional aerodynamics on these results for this low-speed condition. However, the free wake effects are quite noticeable at this low advance ratio. Predicted results with the free wake model show much improved correlation with flight data in terms of harmonic contents, as compared to those obtained with a linear inflow distribution.

Figure 6 shows structural bending for one complete revolution at a 80% radial position. Since three-dimensional aerodynamic effects are small as compared to free wake effects, only two-dimensional aerodynamic results obtained using the free wake are plotted in this figure. Calculated results with the free wake model show improved correlation with data as compared to those with the simplified wake model. The higher harmonic contents in the data are well predicted with the free wake model.

Swept-Tip Blade

Results are calculated for a helicopter blade with a swept-tip planform. The outer 10% of the blade tip is swept back (opposite to rotation) by 30 deg and the same OA209 airfoil shape is used.

The effects of three-dimensional aerodynamics on the vehicle trim solution of the swept-tip blade are summarized in

Table 3 Trim controls of 30 deg swept-tip rotor

	$\mu = 0.14$, $C_T/\sigma = 0.067$			$\mu = 0.387$, $C_T/\sigma = 0.064$		
Pitch Angle	Two-dimensional aero linear wake	Two-dimensional aero free wake	Three-dimensional aero free wake	Two-dimensional aero linear wake	Two-dimensional aero free wake	Three-dimensional aero free wake
θ_0	6.38	6.54	6.76	15.22	15.3	16.42
θ_{1c}	1.03	0.98	0.47	2.83	2.5	2.1
θ_{1s}	1.37	1.79	1.73	−11.27	−11.02	−10.2

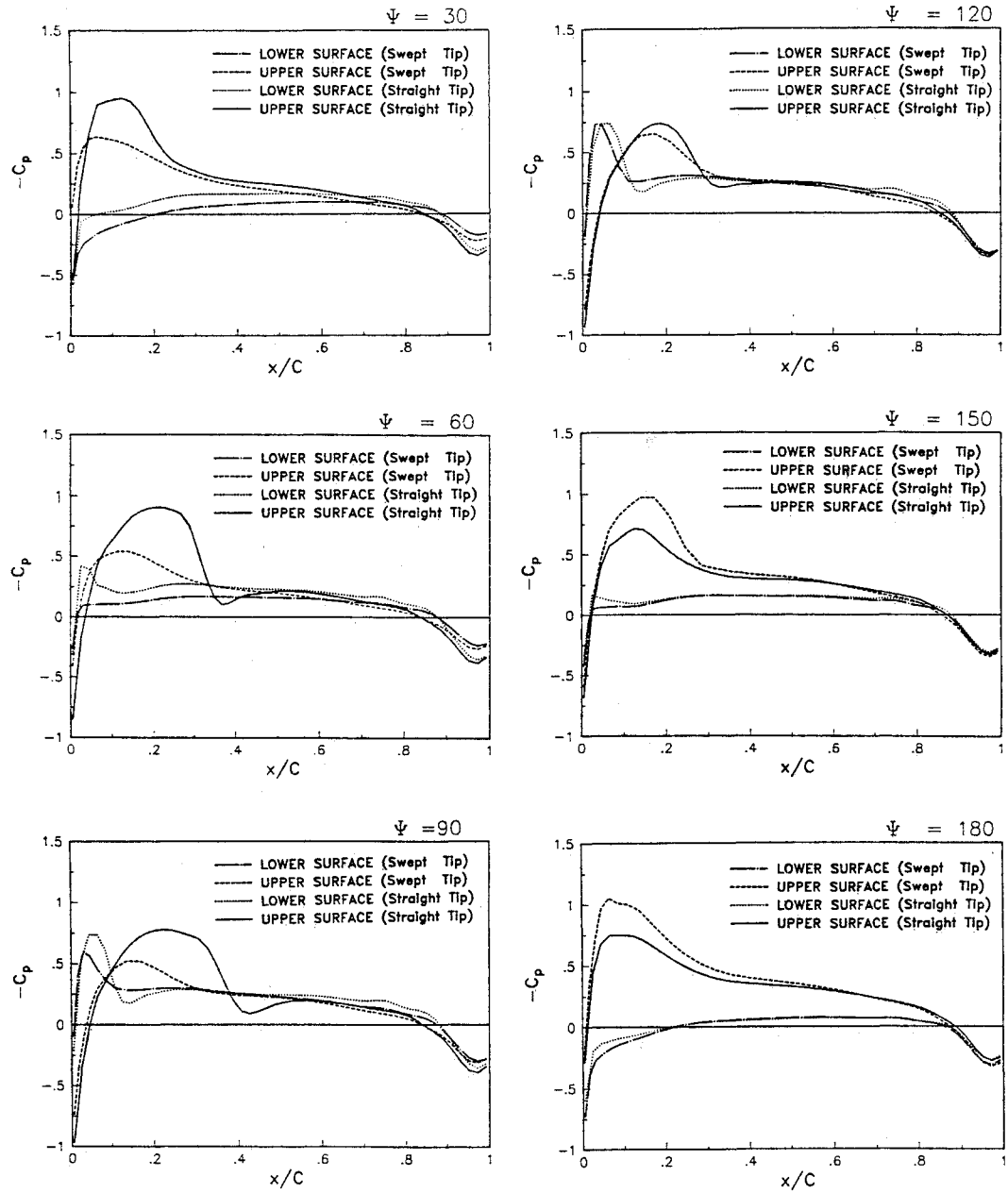

Fig. 9 Pressure distributions of sewpt-tip blade ($\mu = 0.378$, tip sweep = 30 deg, outer 10% R).

Table 3. For comparison purposes, three sets of analytical results are presented: results with two-dimensional aerodynamics and linear inflow; with two-dimensional aerodynamics and free wake; and with three-dimensional aerodynamics and free wake. For the low-speed condition ($\mu = 0.14$), there is a slight difference in collective angle results between two- and three-dimensional calculations, which is also observed in straight-tip results (Table 2). However, the three-dimensional aerodynamic effects on the prediction of lateral cyclic pitch θ_{1c} is quite significant, even for low-speed flight condition. The lateral cyclic pitch obtained using three-dimensional aerodynamics is almost half of that using two-dimensional aerodynamics. This discrepancy is probably due to a large radial flow on the swept tip. For the high-speed condition ($\mu = 0.378$), the three-dimensional effects on the trim solution are quite considerable.

High Forward Speed ($\mu = 0.378$)

Results are presented for a helicopter blade with a swept-tip flying at a high forward speed of $\mu = 0.378$. For this case, a

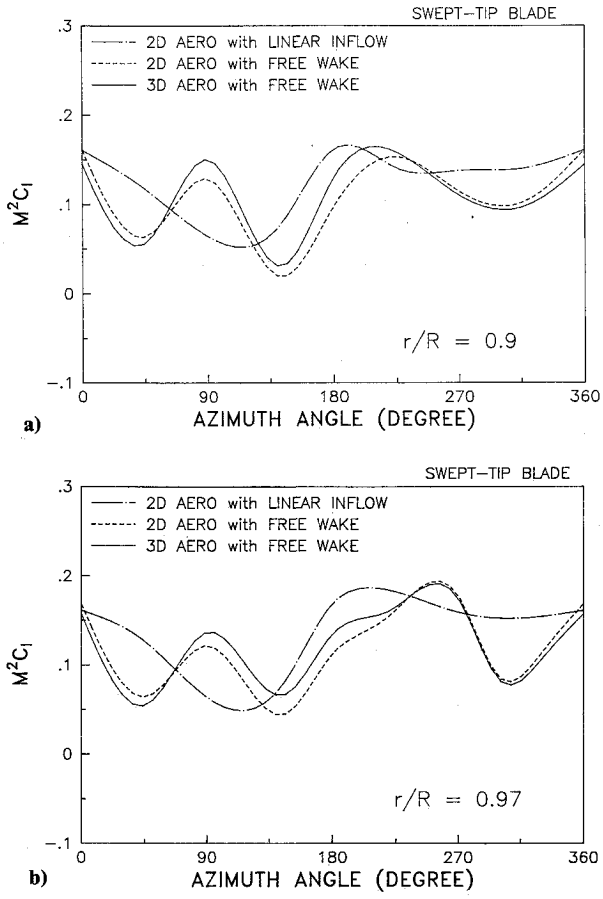

Fig. 10 Lift variations of swept-tip blade (μ = 0.14, tip sweep = 30 deg, outer 10% R): a) Radial station at 0.9R; b) Radial station at 0.97R.

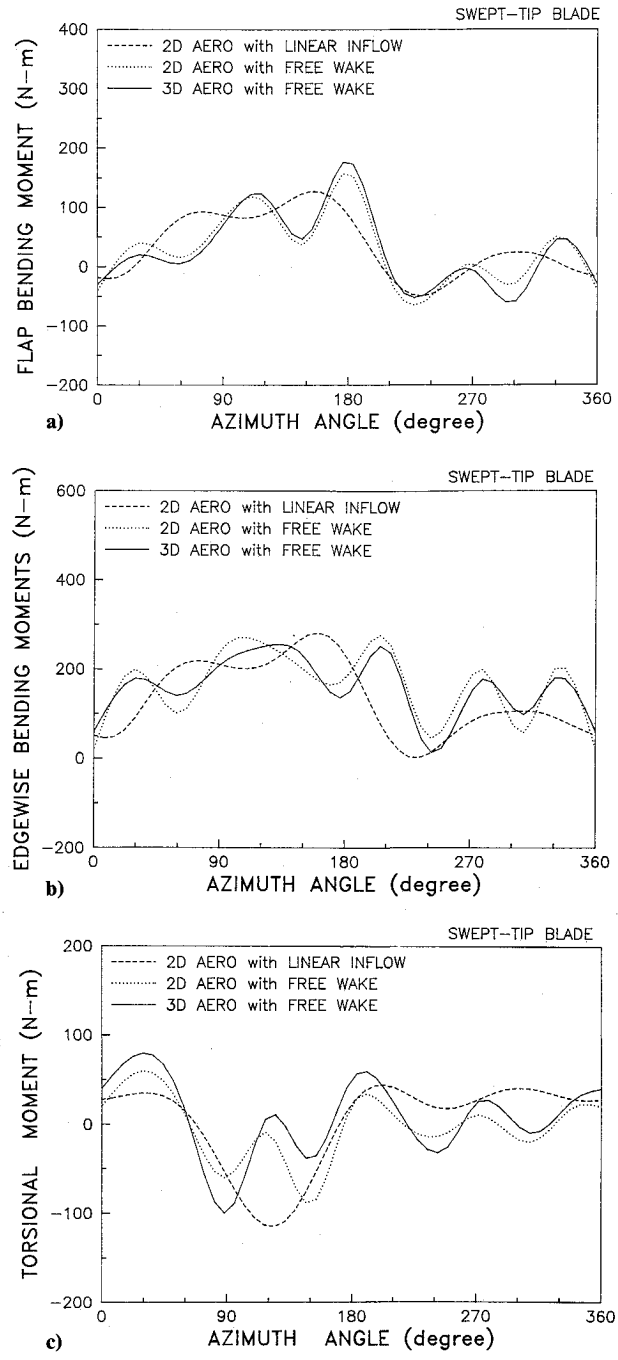

Fig. 11 Structural bendings of swept-tip blade (μ = 0.14, tip sweep = 30 deg, outer 10% R): a) Flap bending moment at 0.8R; b) Lag bending moment at 0.8R; c) Torsional moment at 0.8R.

thrust level C_T/σ of 0.064 is used, and the free wake model is adopted.

Figure 7 presents the lift coefficient variation with azimuth angle for two stations located respectively at 90% (junction) and 97% radial positions. There is a considerable difference in calculated results between two- and three-dimensional aerodynamics, especially at the 97% radial station. As expected, the three-dimensional aerodynamic effects are larger near the tip than at inboard station. The lift variation of the swept blade is somewhat different from that of the straight blade. This is due to two reasons: there is a change in local velocity normal to the blade because of sweep, and a change in aerodynamic pitching moment originating from the aerodynamic center offset from the elastic axis.

Structural bending moments at the 80% radial position for this swept-tip blade are shown in Fig. 8. With three-dimensional aerodynamics, the flap bending moments contain a larger 4/rev vibratory component as compared to the two-dimensional prediction. This is caused by the flap-torsion coupling due to sweep at the tip. Due to large three-dimensional aerodynamic effects on torsional dynamics, the coupling effects are more distinct in the three-dimensional flap bending moment. The effects of three-dimensional aerodynamics on lag bending moments and torsional moments are also significant.

Figure 9 presents the chordwise pressure distributions for the swept-tip blade for a station near the tip (.98R). For comparison, the results from the straight-tip blade are also plotted. It is observed that the intensity of transonic flows is much reduced on the swept-tip blade as compared to the straight-tip results for almost all the advancing side (0 deg < Ψ < 120 deg). But the intensity of shock is slightly increased around Ψ = 150 deg for the swept-tip blade because of delayed supercritical flows, which was also observed in the wind-tunnel test on a isolated swept-tip blade.[16] However, the decrease of transonic flow intensity on the advancing side is certainly the main reason for use of the swept-tip planform for high-speed flight.

Low Forward Speed (μ = 0.14)

Figure 10 presents the variations of lift coefficient with time at 90 and 97% of the radius. For comparison, three sets of analytical results are presented; two-dimensional aerodynamics with linear inflow (Drees), two-dimensional aerodynamics with free wake, and three-dimensional aerodynamics with free wake. Again, the free wake effects are quite noticeable at this low advance ratio, which is also found in straight-tip results. Results with the free wake model contain the high-frequency components as compared to those obtained with a linear in-

flow distribution. It is also observed that unlike straight-tip results, there are some three-dimensional aerodynamic effects shown in this figure. When one looks at the lift variation at the 97% radius (Fig. 10b), one observes noticeable three-dimensional effects on lift, especially around $\Psi = 180$ deg. This is due to high three-dimensionality of swept tip, caused by the radial flow.

Figure 11 shows structural bending for one cycle at a 80% radial position. Again for comparison purposes, three sets of analytical results are presented; two-dimensional aerodynamics with linear inflow (Drees), two-dimensional aerodynamics with free wake, and three-dimensional aerodynamics with free wake. It is observed that the three-dimensional aerodynamic effects are small as compared to free wake effects for this low-speed condition. Structural bending variations of swept-tip blade is quite different from those of straight-tip blade (Fig. 6). When one compares the two-dimensional results alone, there is a 4/rev vibratory component in flap and lag bending moments variations in swept-tip blade, which are not shown in straight-tip results. This is due to strong structural couplings caused by sweep. This points out the importance of accurate dynamic modeling of swept-tip blades.

Conclusions

A new methodology has been developed to study the influence of three-dimensional aerodynamic effects on helicopter response and loads by coupling a rotor dynamic analysis with a three-dimensional finite-difference aerodynamic analysis. The coupling process has been done in a consistent manner by using the calculated three-dimensional lift and moment characteristics from a CFD code in the dynamic analysis prediction. Trimmed control values and elastic rotor response are updated including three-dimensional aerodynamic effects. Analytical results are correlated with the flight-test data obtained on a SA349/2 Gazelle helicopter. The following conclusions are drawn from this study:

1) For the trim solution, predicted and measured values for collective pitch agree very well, although there are some differences for the cyclic pitch. Inclusion of three-dimensional aerodynamic effects generally helps the correlation for trim controls.

2) For a low forward flight condition ($\mu = .14$), the wake plays a dominant role as compared to three-dimensional aerodynamic effects on blade response and loads. Using a refined wake model helps to improve the rotor loads correlation.

3) For a high forward speed condition ($\mu = .378$), there is a considerable influence of three-dimensional aerodynamics on blade response and loads. The correlation of aerodynamic loads is improved with the inclusion of three-dimensional aerodynamics, particularly near the outboard section of the blade.

4) Inclusion of three-dimensional effects in pitching moment appears quite large and helps to improve the correlation for torsional moment in the high-speed case.

5) For a swept-tip blade, the intensity of transonic flows on the advancing side is much reduced as compared to the straight-tip result.

6) The effects of tip sweep on the blade structural bending moments are quite large in the high-speed case.

This paper is a step toward the development of an advanced comprehensive helicopter analysis encompassing current advances in both structural and aerodynamic modeling. In spite of it being computer intensive, its benefits must be appreciated as a powerful tool to validate simple design-oriented analyses.

Acknowledgments

This research work was supported by the Army Research Office, Contract No. DAAL-03-88-C002; Technical Monitor, Tom Doligalski. Authors would like to express appreciation to Andre Desoper (ONERA) for his many valuable discussions.

References

[1]Kim, K. C., Desopper, A., and Chopra, I., "Dynamic Blade Response Calculations Using Improved Aerodynamic Modeling," *Journal of the American Helicopter Society,* Vol. 3b, Jan. 1991, pp. 68–77.

[2]Yamauchi, G. K., Heffernan, R. M., and Gaubert, M., "Correlation of SA349/2 Helicopter Flight Test Data with a Comprehensive Rotorcraft Model," *Journal of the American Helicopter Society,* Vol. 33, April 1988, pp. 32–42.

[3]Celi, R., and Friedmann, P. P., "Aeroelastic Modeling of Swept Tip Rotor Blades Using Finite Elements," *Journal of the American Helicopter Society,* Vol. 33, April 1988, pp. 43–52.

[4]Benquet, P., and Chopra, I., "Calculated Dynamic Response and Loads for an Advanced Tip Rotor in Forward Flight," *Proceedings of the 15th European Rotorcraft Forum,* Amsterdam, Sept. 1989.

[5]Heffernan, R. M., and Gaubert, M., "Structural and Aerodynamic Loads and Performance Measurements of an SA349/2 Helicopter with an Advanced Geometry Rotor," NASA TM 88370, Nov. 1986.

[6]Kim, K. C., "Dynamic Analysis of Advanced Tip Rotors including Three-Dimensional Aerodynamics," Ph.D. Thesis, Department of Aerospace Engineering, Univ. of Maryland at College Park, July 1990.

[7]Sivaneri, N. T., and Chopra, I., "Finite Element Analysis for Bearingless Rotor Blade Aeroelasticity," *Journal of the American Helicopter Society,* Vol. 29, April 1984, pp. 42–51.

[8]Dull, A. L., and Chopra, I., "Aeroelastic Stability of Bearingless Rotors in Forward Flight," *Journal of the American Helicopter Society,* Vol. 33, Oct. 1988, pp. 38–46.

[9]Lim, J. W., and Chopra, I., "Response and Hub Loads Sensitivity Analysis of a Helicopter Rotor," *AIAA Journal,* Vol. 28, Jan. 1990, pp. 75–82.

[10]Kim, K. C., Bir, G., and Chopra, I., "Helicopter Response To An Airplane's Vortex Wake," *Vertica,* Vol. 12, No. 1/2, 1988, pp. 39–54.

[11]Panda, B., and Chopra, I., "Dynamics of Composite Rotor Blades in Forward Flight," *Vertica,* Vol. 11, No. 1/2, 1987, pp. 187–209.

[12]Panda, B., "Technical Note: Assembly of Moderate-Rotation Finite Elements Used in Helicopter Rotor Dynamics," *Journal of the American Helicopter Society,* Vol. 32, Oct. 1987, pp. 63–69.

[13]Johnson, W., "A Comprehensive Analytical Model of Rotorcraft Aerodynamics and Dynamics, Part I: Analysis Development," NASA TM-81182, June 1980.

[14]Johnson, W., "Assessment of Aerodynamic and Dynamic Models in a Comprehensive Analysis for Rotorcraft," *Computers and Mathematics with Applications,* Vol. 12A, Jan. 1986, pp. 11–28.

[15]Chattot, J., "Calculation of Three Dimensional Unsteady Flow Past Helicopter Blades," NASA TP-1721, 1980.

[16]Desopper, A., "Study of Unsteady Transonic Flow on Rotor Blade with Different Tip Shapes," *Vertica,* Vol. 9, 1985, pp. 257–272.

[17]Desopper, A., Lafon, P., Ceroni, P., and Philippe, J. J., "Ten Years of Rotor Flow Studies at ONERA," *Journal of the American Helicopter Society,* Vol. 34, Jan. 1989, pp.34–41.

[18]Caradonna, F. X., Desopper, A., and Tung, C., "Finite Difference Modeling of Rotor Flows including Wake Effects," *Proceedings of the 8th European Rotorcraft Forum,* Aix-en-Provence, France, Aug. 1982.